The three-dimensional wake of a cylinder undergoing a combination of translational and rotational oscillation in a quiescent fluid

M. Nazarinia, D. Lo Jacono, M. C. Thompson, and J. Sheridan
Department of Mechanical and Aerospace Engineering, Fluids Laboratory for Aeronautical and Industrial Research (FLAIR), Monash University, P.O. Box 31, Melbourne, Victoria 3800, Australia

(Received 18 February 2009; accepted 5 May 2009; published online 4 June 2009)

Previous two-dimensional numerical studies have shown that a circular cylinder undergoing both oscillatory rotational and translational motions can generate thrust so that it will actually self-propel through a stationary fluid. Although a cylinder undergoing a single oscillation has been thoroughly studied, the combination of the two oscillations has not received much attention until now. The current research reported here extends the numerical study of Blackburn *et al.* [Phys. Fluids **11**, L4 (1999)] both experimentally and numerically, recording detailed vorticity fields in the wake and using these to elucidate the underlying physics, examining the three-dimensional wake development experimentally, and determining the three-dimensional stability of the wake through Floquet stability analysis. Experiments conducted in the laboratory are presented for a given parameter range, confirming the early results from Blackburn *et al.* [Phys. Fluids **11**, L4 (1999)]. In particular, we confirm the thrust generation ability of a circular cylinder undergoing combined oscillatory motions. Importantly, we also find that the wake undergoes three-dimensional transition at low Reynolds numbers ($\mathrm{Re} \simeq 100$) to an instability mode with a wavelength of about two cylinder diameters. The stability analysis indicates that the base flow is also unstable to another mode at slightly higher Reynolds numbers, broadly analogous to the three-dimensional wake transition mode for a circular cylinder, despite the distinct differences in wake/mode topology. The stability of these flows was confirmed by experimental measurements. © *2009 American Institute of Physics*.
[DOI: 10.1063/1.3147935]

I. INTRODUCTION

A circular cylinder undergoing a combination of oscillatory translation and rotation in quiescent fluid has not received much attention until now. It is well known that when a bluff body is oscillating translationally in a quiescent fluid, secondary streaming is generated around the body because of nonlinear effects.[1] However, the combination of two oscillatory forcing mechanisms, under specific conditions detailed later, results in a net thrust being experienced by the circular cylinder in a direction normal to the translational axis.[2] The cylinder experiencing thrust, while undergoing a series of pitch and plunge, has been labeled the *swimming cylinder*.

Numerous studies involving pure oscillatory motions, either translational or rotational, exist for different flow conditions.[3–13] Among them Honji[3] for the first time produced visualizations of the three-dimensional structures of such flows. Honji[3] visualized the flow around a transversely oscillating cylinder in a quiescent fluid, and produced excellent visualizations of a three-dimensional flow instability. The presence of mushroom shaped vortices was observed, in a plane normal to the direction of cylinder motion, which was arranged alternately along each side of the cylinder span in a double row. These structures were named the "Honji instability" by Sarpkaya[14] although Honji simply referred to the patterns formed as "streaked flow." Also Tatsuno and Bearman[5] produced a control space map, classifying the space into eight flow regimes each with a two- or three-dimensional flow structure and vortex shedding characteristics. Using two different flow visualization techniques, they comprehensively investigated translational harmonic oscillation in a quiescent fluid over a range of two independent variables, e.g., the amplitude and frequency of oscillation.

More recent numerical works[15–17] studied the instability of such flows, as well as Nehari *et al.*[18] who numerically looked at three dimensionality of the flow at low amplitudes and frequencies. Elston *et al.*[15,16] investigated the wakes using direct numerical simulation with Floquet analysis. They isolated and classified the symmetry breaking instabilities from the two-dimensional basic states as a function of Tatsuno and Bearman's[5] control parameters.

Although not strictly relevant to the present study being in a quiescent fluid, the flows around a rotationally oscillating cylinder have also been investigated thoroughly.[9–13,19,20] Taneda[9] experimentally investigated the effects of rotary cylinder oscillations over a low Reynolds number range ($\mathrm{Re}=[30-300]$) using flow visualization. Experiments at a higher Reynolds number[10] of 1.5×10^4 have yielded related results to those of Taneda.[9] Numerical studies of vortex shedding from a rotationally oscillating cylinder,[19,20] recorded the transition and selection of different vortex shedding modes and the lock-on phenomenon. More recently, Poncet[11] looked at the three dimensionality of flow around a cylinder undergoing rotational oscillation.

So far, to the best knowledge of the authors, only the investigations by Blackburn *et al.*[2] and more recent ones[21–24]

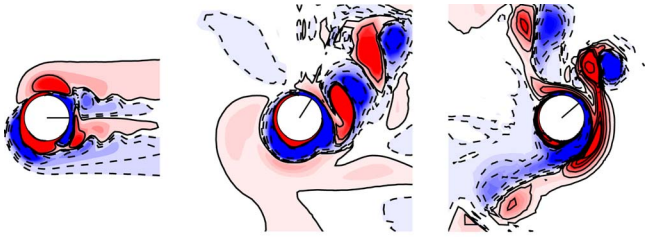

FIG. 1. (Color online) Contours of vorticity around the cylinder undergoing combined translational and rotational oscillation at $KC=\pi$, $\beta=90$, and (a) $\Phi=\pi$, (b) $\Phi=\pi/2$, (c) $\Phi=\pi/4$, taken at $t/T=0$ from numerical simulation. The dashed lines (enclosing blue) correspond to clockwise direction of vorticity (negative). The solid lines (enclosing red) correspond to counterclockwise direction of vorticity (positive).

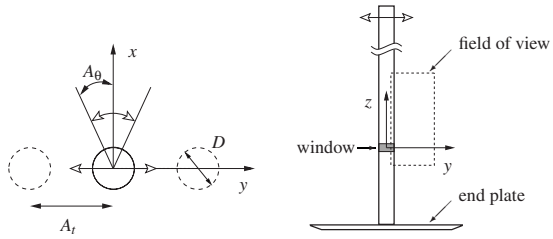

FIG. 2. Schematic of the problem geometry and important parameters relevant to the combined forcing. Left: the two-dimensional overview (xy-plane) of the cylinder. Right: spanwise view of the cylinder (yz-plane) with end plate and field of view (PIV).

reported on the combined oscillatory motion of a cylinder. Among them the work by Blackburn *et al.*[2] is the only one on the swimming cylinder (i.e., the quiescent case). A number of interesting features have been shown to occur as a result of combining the two motions. Of principal interest is the jet flow produced by the cylinder when the two imposed motions are in opposition of phase. The propulsive force produced by the cylinder causes it to accelerate until eventually reaching a terminal speed of 33% of the peak translational speed.[2] Naturally, the above mentioned phenomena is also true when the two motions are in phase, the difference being the side where the jet flow is produced. The combination of oscillatory motions has also been shown to be capable of producing a wide variety of flow patterns depending on the phase. Figure 1 shows an example of the near wake structure for a different phase. It can be seen that by changing the phase angle, the flow field around the cylinder changes dramatically. Notably it is clear that only the in phase or opposing phase cases ($\Phi=0,\pi$) produce a jetlike flow. The other phases result in a flow with a somewhat preferred direction without the jetlike feature. The results by Blackburn *et al.*[2] were obtained via numerical simulations but to date, no detailed experimental studies into the effect of combining an oscillatory rotational and translational motion of a circular cylinder in either quiescent fluid or in external flow are known. However, a similar form of motion, *Carangiform motion*, is observed in nature. This mode of oscillation necessitates a twist at each extreme of the oscillation to give backward inclination to the moving winglike surface, that is, to a vertically oscillating cetacean tail, or to a fish's horizontally oscillating caudal fin. However, the propulsive jet that is produced from Carangiform motion only occurs when the oscillations are in phase.[25] The purpose of the present study is to investigate not only the near wake structure of such a combination of forcing mechanisms, but also to extend this to examine the three-dimensional nature of the wake, which is yet to receive any attention. The present study incorporates both experimental and numerical results. To characterize the experimental flows, the authors employed particle image velocimetry (PIV). Direct numerical simulation and Floquet analysis are also used to provide further insight in the wake flows produced. In Secs. II–IV, after defining the problem under investigation, the experimental and numerical techniques utilized are described. Some validation with previous studies is then presented. The results and discussion sections follow, ending with conclusions.

II. PROBLEM DEFINITION

When the relative flow past a cylinder is undergoing combined sinusoidal translational and rotational oscillations, the structure of the flow generated by the cylinder depends mainly on five independent parameters. The equations of the forcing motion are defined as

$$y(t) = A_t \sin(2\pi f_t t), \tag{1}$$

$$\theta(t) = A_\theta \sin(2\pi f_\theta t + \Phi), \tag{2}$$

where A_t (A_θ) is the amplitude of the translational (rotational) motion, f_t (f_θ) is the frequency of translational (rotational) oscillation, and Φ is the phase between rotational and translational motions.

The dimensionless quantities representative of amplitude and frequency of each motion are usually defined as follows:

$$KC_t = \frac{U_{\max_t}}{f_t D} = \frac{2\pi A_t}{D}, \quad KC_\theta = \frac{U_{\max_\theta}}{f_\theta D} = \pi A_\theta, \tag{3}$$

$$\beta_t = \frac{f_t D^2}{\nu}, \quad \beta_\theta = \frac{f_\theta D^2}{\nu}, \tag{4}$$

where KC_t (KC_θ) and β_t (β_θ) are the translational (rotational) Keulegan–Carpenter number and Stokes number, respectively; $U_{\max_t}$ ($U_{\max_\theta}$) is the maximum translational (rotational) velocity of the cylinder motion, D is the cylinder diameter, and ν is the kinematic viscosity of the fluid.

A Reynolds number can also be defined as a combination of two of the above dimensionless parameters. The associated translational Reynolds number, Re_t, is then

$$\mathrm{Re}_t = \frac{U_{\max_t} D}{\nu} = KC_t \beta_t. \tag{5}$$

Figure 2 shows a schematic of the problem studied with some relevant notations and features. The Cartesian coordinate system in use is defined such that the origin is located at the center of the circular cylinder (at $t=0$) at the window shown in Fig. 2, with x, y, and z representing the streamwise, transverse, and spanwise directions, respectively (see Fig. 2).

III. METHODS AND TECHNIQUES

A. Experimental setup

The experiments were conducted in the FLAIR free-surface closed-loop water channel at the Department of Mechanical and Aerospace Engineering, Monash University. Experiments were performed for a particular set of parameters which was shown earlier to be that of a swimming cylinder:[2] The frequency ratios were held to be the same $\beta_t=\beta_\theta=\beta$ and the phase difference between the two motions set to $\Phi=\pi$. The associated translational and rotational Keulegan–Carpenter numbers are $KC_t=KC_\theta=\pi$. The nondimensional frequency was chosen to cover the range $45\leq\beta\leq200$, consequently the range of Re_t covered was $141\leq\mathrm{Re}_t\leq628$.

The experimental model used for these experiments was a hollow circular cylinder of length 800 mm and outer diameter 20 mm, giving an aspect ratio of 40, see Fig. 2. The cylinder was made of carbon fiber and suspended vertically from an actuator that was controlled by a microstepping stepper motor. The cylinder was fitted with an end plate to reduce the end effects. The end plate was designed following recommendations by Stansby[26] and consisted of a circular plate with a diameter of $9D$. For PIV purposes, a small section of the cylinder was replaced by a thin-walled transparent cylinder, whose interior was filled with distilled water. The results shown later in the xy-plane are taken through this window.

The cylinder was oscillated translationally and rotationally by using two high-resolution stepper motors. The translational stepper motor actuated the rodless in-line mounting actuator and the rotational stepper motor was connected directly to the vertically mounted cylinder. The stepper motors were controlled using a two-axis indexer and two high-resolution drivers (running at 50 800 steps rev^{-1}). A pure sinusoidal profile, as defined in Eqs. (1) and (2), was used throughout the paper. A TTL-signal triggered other devices (camera and laser), thus images could be captured at preselected phase angles in the oscillation cycle (phase locked).

During each set of experiments the fluid was initially at rest, i.e., it was *quiescent*. Special care was always taken to ensure near quiescency of the flow. Prior to each set of experiments, a honeycomb device was drawn through the working volume to break up large-scale flow structures into smaller scales, minimizing the time required to reach the background noise level. Typically, this background level, measured by the norm of velocity magnitude, was kept less than 1.41% of $U_{\max_t}$ (0.1 mm s^{-1} or less).

B. Experimental techniques

The velocity vector fields around the combined oscillating circular cylinder were measured using PIV. The PIV setup, illustrated schematically in Fig. 2, was based on that originally described by Adrian[27] and developed in-house over the past decades. The flow was seeded with spherical polyamide particles with a mean diameter of 20 μm and specific weight of 1.016 g cm^{-3}. In this system, the particles were illuminated using two miniature Nd:YAG (yttrium aluminum garnet) laser sources (Continuum Minilite II Q-Switched). The planes of interest for these experiments were the yz- and xy-planes, being the spanwise and streamwise directions, as shown in Fig. 2. The thickness of the laser sheet was measured to be approximately less than 2 mm. Pairs of images were captured on a high-resolution charge coupled device camera with a maximum resolution of 4008×2672 pixels. The camera was equipped with a 105 mm lens (Nikon Corporation, Japan). At a particular phase of the oscillation cycle, a number of image pairs over successive cycles were taken and stored for further processing. The timing of the laser and camera triggering was controlled by a special in-house designed timing unit, with an estimated accuracy of 1 μs.

Each image pair was processed using in-house PIV software.[28] This software uses a double-frame, cross-correlation multiwindow algorithm to extract a grid of displacement vectors from the PIV images. An interrogation window of 32×32 (with an initial window size of 64×64) pixels was found to give satisfactory results with 50% overlap. More than 98% of the vectors were valid for all the experiments. This window size corresponds to an average interrogation window of $0.064D\times0.064D$. It was possible to obtain a measurement resolution of 249×166 (total of 41334) vectors in each field of view. The overall field of view was 4008×2672 pixels ($8.0D\times5.3D$).

Phase-averaged vorticity and velocity fields are presented using 30 or more instantaneous measurements. The vorticity fields were calculated with the technique described previously.[29] The velocity and spatial coordinates are nondimensionalized by the maximum velocity of the translational cylinder motion, $U_{\max_t}$, and the cylinder diameter, D, respectively.

Our PIV setup and technique have been validated against the previous numerical and experimental results[5,8] for the xy- and yz-plane measurements. The validation case studied is for a purely translational oscillation in a quiescent fluid. Figure 3 demonstrates an excellent agreement with the experimental and numerical study by Dütsch *et al.*[8] The numerical results (explained in Sec. III C) also match well with those of Dütsch *et al.*[8] Other profiles (not shown) at different locations are also in good agreement. For three-dimensional validation, the measured spanwise wavelength ($\lambda=1.04D$) for the $KC_t=2.51$ and $\beta_t=142$ ($\mathrm{Re}_t=356$) case, corresponding to regime B of Tatsuno and Bearman[5] control parameter map (Fig. 12 of Ref. 5), was found to be within 4% of the previously reported value[5] ($\lambda\approx1.0D$), where λ is the wavelength along the span of the cylinder.

C. Numerical formulation

The description of the methodology will be purposefully brief because of descriptions given in previous papers. Details of the method in general,[30] and details of the implementation used here[31] can be found elsewhere. The code employed has been well proven for use in bluff-body problems, and Floquet stability analysis.[17,32–34] However, a brief outline of the method is given. The base flows for the present study were calculated by solving the incompressible, time-dependent Navier–Stokes equations. The discretization

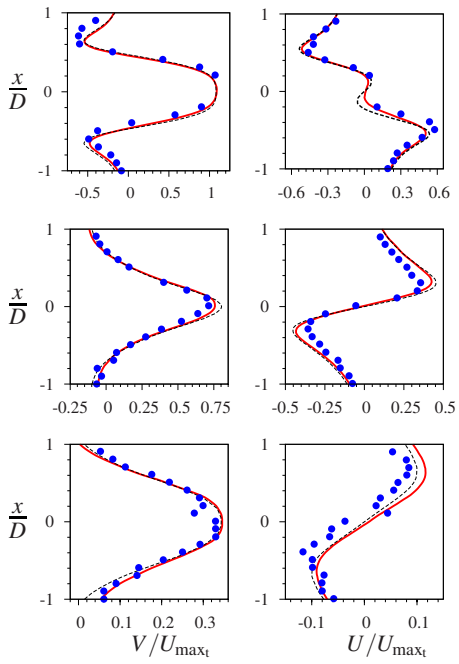

FIG. 3. (Color online) Comparison of the velocity components at three cross sections of the translationally oscillating cylinder in a quiescent fluid at constant y/D values. The y/D values from the top to bottom rows are -0.6, 0.6, and 1.2, respectively. The measurements are taken at $KC_t=5$ and $\beta_t=20$, similar to previous numerical and experimental results (Ref. 8). The left column depicts the $V/U_{\max_t}$ and the right column $U/U_{\max_t}$. The solid lines (red) show the present experiment, the dashed lines (black) the present numerical simulation and the filled circle points (blue) the experimental results of Dütsch *et al.* (Ref. 8).

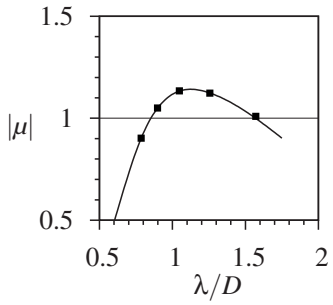

FIG. 4. Floquet multipliers for $KC_t=2.75$ for the three-dimensional instability of regime B at $\beta_t=80$. The current results (solid line) are compared to those from Elston *et al.* (Ref. 16) (squares).

method employed was a spectral-element method, using seventh-order Lagrange polynomials associated with Gauss–Lobatto–Legendre quadrature points. The time integration was executed using a three-step splitting scheme.[35–37] A computational domain extending $30D\times30D$ was split into 518 elements, the majority of which were concentrated in the boundary layer. The resolution, element distribution and domain size are consistent with those used successfully in previous similar studies. At the cylinder surface, a time-dependent Dirichlet condition was utilized that varied sinusoidally in time according to the driven translational and rotational oscillations. The calculations were performed in an accelerating frame of reference attached to the cylinder. The frame acceleration was added to the Navier–Stokes equations to account for this. The method employed is second order in time and time stepping is governed by the Courant condition on the explicit convective substep. The unit time step employed was 0.010 ($\approx$1250 time step/cycle) for $\beta\leq70$ and 0.005 ($\approx$2500 time step/cycle) for $\beta>70$.

Floquet stability analysis employing a power method to resolve the most dominant Floquet mode (and the magnitude of the largest Floquet multiplier) has been used. Floquet stability analysis is a linear method designed to deduce the stability of periodic systems. The stability is deduced by calculating the *Floquet* multiplier, μ, which can be thought of as the ratio of growth in amplitude of a perturbation from one period to the next, for a perturbation of a given spanwise wavelength, λ/D. If this ratio is such that $|\mu|>1$, then the perturbation grows each period, and the two-dimensional base flow is said to be unstable to three-dimensional perturbations. Conversely, if $|\mu|<1$, the perturbation decays each period, and will eventually die away, meaning the base flow is stable. Generally, this relies on the fact that a random perturbation of a given wavelength can be decomposed into a summation of eigen- or Floquet modes, each of which grows or decays at a certain rate. It is the fastest-growing or slowest decaying Floquet mode—the dominant mode—which dominates asymptotically with time. That is, after a certain amount of time, a perturbation decays to the dominant Floquet mode, with the size of the Floquet multiplier relative to unity determining the stability of the base flow. Details of the formulation can be found elsewhere.[38]

Figure 4 shows a validation of our technique with previous numerical simulations.[16] The validation case studied is a pure translational motion with $KC_t=2.75$ and $\beta_t=80$ ($\mathrm{Re}_t=220$), corresponding to regime B.[5] The agreement was found to be excellent throughout the range tested.

IV. RESULTS AND DISCUSSION

In this section the results are presented in two parts. For the first, the wake profiles around the cylinder in the streamwise direction (xy-plane) for $KC=\Phi=\pi$ and $\beta=90$ are examined, and the second part investigates the three dimensionality of such flows for $KC=\Phi=\pi$ and a range of $20<\beta<200$ (corresponding to $62.8<\mathrm{Re}_t<628$).

A. Wake profile in the streamwise direction

It has previously been found that for the case where $KC=\Phi=\pi$ and $\beta=90$, while the cylinder translation axis is vertical, vorticity transport is predominantly in the horizontal direction.[2] Figure 5 clearly shows this vorticity transport to one side of the cylinder as well as comparing the same flow between the present experimental and numerical investigation. Figure 5 also shows the excellent qualitative agreement between the two methods used. Figure 6 depicts the sequence of one complete cycle of translational and rotational oscillation. The cylinder motion, based on Eqs. (1) and (2), starts from the center toward the top of the page, the positive direction of y, and at the same time starts rotating clockwise, the negative direction of rotation angle, θ. Figure 6(c) shows the instant when the cylinder is at its maximum vertical po-

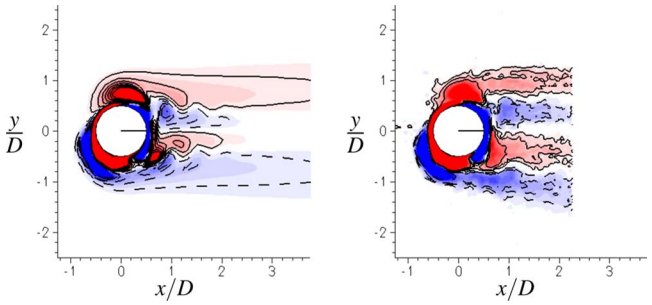

FIG. 5. (Color online) Vorticity contours around the cylinder undergoing combined translational and rotational oscillation at $KC=\Phi=\pi$ and $\beta=90$. The numerical result is presented at the left, and the experimental result at the right. The experimental result is a phase-average of ten successive cycles. The phase shown corresponds to $t=0$. The dashed lines (enclosing blue) correspond to clockwise direction of vorticity (negative), and the solid lines (enclosing red) corresponds to counterclockwise direction of vorticity (positive).

sition and most negative angular displacement. As the oscillations are in opposition of phase, the maximum surface-tangential component of cylinder acceleration is located on the left-hand side of the cylinder, i.e., it is where the accelerations are additive rather than in opposition. Morton[39] showed that this combination of accelerations will result in the (kinematic) generation of vorticity on that side of the cylinder while the cancellation of accelerations on the other side results in little direct vorticity generation on the right side. The direction of rotation of the vortices will result in their being strained and directed to only one side of the cylinder and perpendicular to its translation axis. Based on the vorticity fields, this will necessarily result in thrust generation in this direction, but it has not been effectively measured experimentally. The thrusting effect appears to occur in a lock-in regime and, as reported earlier,[2] would be expected to occur for all cases where the flow structure is as shown in Fig. 1(a). However, it may be the case that there is a threshold set of amplitudes required to establish this but that has not been determined to date. The phase angle between the motions influences the degree to which cross annihilation of vorticity occurs and the distance from the cylinder at which vorticity persists (as was shown in Fig. 1).

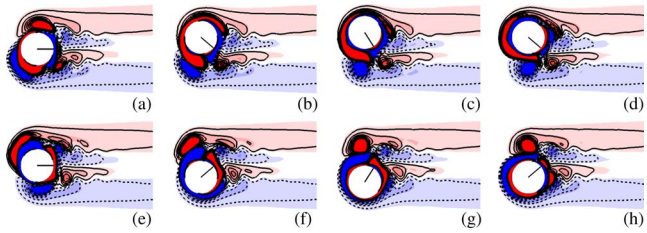

FIG. 6. (Color online) Flow produced by a cylinder with combined oscillatory translation and rotation. This figure shows the sequence and development of the ω_z vorticity for one complete cycle, (a) $t=0$ to (h) $t=7T/8$ at $KC=\Phi=\pi$ and $\beta=90$, where T is the period of oscillation. The radial line shows the rotational displacement of the cylinder. The dashed lines (enclosing blue) correspond to clockwise direction of vorticity (negative), and the solid lines (enclosing red) correspond to counterclockwise vorticity (positive).

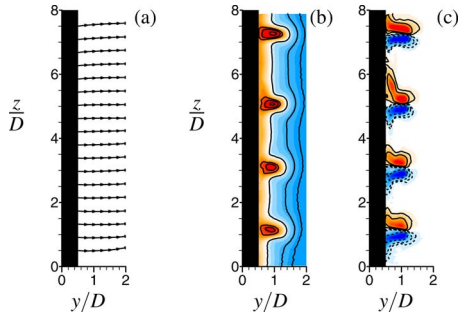

FIG. 7. (Color online) Experimental results of the spanwise distribution of flow for two values of β at $KC=\Phi=\pi$: (a) $\beta=20$, streamlines; (b) $\beta=90$, u_y velocity isocontours; (c) $\beta=90$, ω_x vorticity isocontours; the dashed lines (enclosing blue) correspond to clockwise direction of vorticity (negative), and the solid lines (enclosing red) correspond to counterclockwise vorticity (positive).

B. Wake profile in the spanwise direction

Figure 7 shows the experimental spanwise distribution of flow for two values of β at $KC=\Phi=\pi$. Figure 7(a) shows approximately parallel streamlines indicating two-dimensional vortex shedding around the cylinder. Here $\mathrm{Re}\approx 63$, which the Floquet analysis, discussed later, shows to be a two-dimensional flow regime. Figures 7(b) and 7(c) present the y-velocity field (u_y) and vorticity field (ω_x) contours along the span of cylinder, respectively. These are for $\mathrm{Re}\approx 283$. The spanwise three-dimensional structures are clearly seen from these two depictions. The three-dimensional structures shown appear regular and stable, with a constant characteristic wavelength. Further analysis of the experimental data, not presented here, shows this to be the case.

Figure 8 shows the Floquet multipliers, $|\mu|$, for several Reynolds numbers for a spanwise instability at $KC=\Phi=\pi$. Figure 8(a) shows the value of $|\mu|$ as a function of the spanwise wavelength, λ/D. This figure clearly depicts the emergence of two distinct instability modes, a short and a long

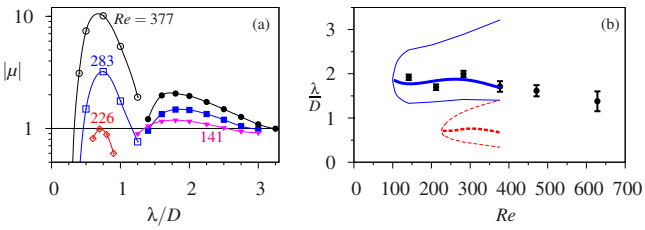

FIG. 8. (Color online) Floquet multipliers for several Reynolds numbers for the spanwise instability at $KC=\Phi=\pi$. (a) Floquet multipliers as a function of spanwise wavelength. The open (closed) symbols represent the shortest (longest) wavelength mode. The circles and black line represent results for Re=377; the squares and blue line represent results for Re=283; the diamonds and red line represent results for Re=226; the lower triangles and magenta line represent results for Re=141. (b) Comparison of the Floquet analysis predicted wavelength values as a function of Reynolds number with experimental measurements. The blue dashed line corresponds to the wavelength range of the longest spanwise wavelength mode. The red dashed dotted line corresponds to the extent of the shortest spanwise wavelength mode. The thick blue and red lines correspond to the predicted values of the long and short wavelengths, respectively. The black circles represent the present experimental measurements with error bars reporting the standard deviation of the measurements.

wavelength mode. The longer wavelength mode has a critical Reynolds number of $\mathrm{Re}_c \approx 100$, at a critical wavelength of $\lambda \approx 1.8D$. The second instability first occurs at a much higher Reynolds number of $\mathrm{Re}_c \approx 226$ for a wavelength of $\lambda \approx 0.7D$. The experiments show that the spanwise wavelength observed in the wakes at various Reynolds numbers was close to $2D$ at onset, decreasing to about $1.5D$ at $\mathrm{Re}=600$. These values are consistent with the wavelengths corresponding to the fastest-growing modes as the Reynolds number is varied. This is clearly depicted in Fig. 8(b), which shows the unstable Reynolds number range for each mode as a function of Reynolds number and the preferred wavelength. The experimental wavelength variation with Reynolds number matches the predicted preferred wavelength reasonably well.

These long and short wavelength modes have the same spatiotemporal symmetries as modes *A* and *B* wake modes for a stationary circular cylinder in a uniform flow,[40] respectively. These symmetry breaking bifurcations are the only ones possible with the same period as the base flow, as shown using group theory arguments by Blackburn *et al.*[41] It is interesting to note that the symmetry breaking transitions occur in the same order as for a circular cylinder, even though the two-dimensional base wake flow and perturbation field distributions are completely different. Of course, for different body geometries, the transition order can be different, such as for an elongated streamlined leading-edge square trailing-edge cylinder, for which the transition order is reversed.[33] Perhaps of even more interest is that for a circular cylinder wake, the saturated second critical mode, mode *B*, dominates the flow dynamics as the Reynolds number is increased above the two transitions;[42] in fact, for Reynolds numbers close to 300, the wake appears to be in an almost pure mode *B* state.[43] Notably this corresponds to the Reynolds number at which mode *B* growth rate grows to exceed that of mode *A*. This is not the case here. Despite examining the wakes experimentally at Reynolds numbers up to 640, there was no sign of any evidence of the shorter wavelength instability in the wake. There was also an attempt to artificially force the wake at this wavelength by placing thin tapes on the cylinder spaced at the predicted optimal shorter wavelength. This also failed to generate any long term change to the wake, i.e., the shorter wavelength mode was visible initially but the wake quickly reverted to the longer wavelength state, similar to that shown in Fig. 7 for the unperturbed case. Figure 8(a) clearly shows that linear theory predicts the growth rate of the shorter wavelength mode quickly overtakes the longer wavelength mode, so this is somewhat surprising. Of course, the growth and nonlinear saturation of the long wavelength mode changes the base flow so this result is not inconsistent.

Figure 9 shows the perturbation ω_z vorticity contours of the short and long wavelength modes associated with the spanwise instability. This clearly shows the spatiotemporal symmetries of the two modes: In terms of the perturbation vorticity, for the long wavelength mode, the field repeats on passage in time through half a period, reflection about the centerline and reversal of sign, while for the shorter wavelength mode the sign reversal is not required. These symmetries are the same as for modes *A* and *B*, respectively. The mode structure of both modes is quite complex, with substantial mode amplitude both near the cylinder and in the wake.

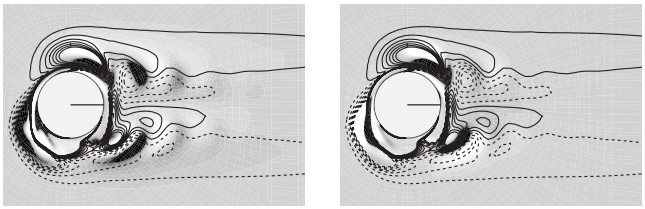

FIG. 9. Contours of streamwise perturbation vorticity taken at $KC=\Phi=\pi$ and $\beta=90$ ($\mathrm{Re}\approx 283$) and when the cylinder is at $t=0$ for the following: (left) $\lambda=1.8D$ the long wavelength; (right) $\lambda=0.7D$ the short wavelength. The dashed lines correspond to the base flow clockwise direction of vorticity (negative), and the solid lines correspond to the counterclockwise vorticity (positive).

V. CONCLUSIONS

In this work we have experimentally and numerically considered the development of three dimensionality of flow around a cylinder undergoing a combined translation and rotation oscillatory motion. The study is restricted to the case with the phase angle set to π, and large amplitude oscillations—corresponding to a *swimming cylinder*. Because of this phase difference, the oscillation velocities at the cylinder surface cancel on one side and reinforce on the other. This leads to preferential vorticity generation and transport on one side, and the cylinder rotational motion sweeps this vorticity around to the other side producing a thrust wake. Although previous two-dimensional simulations have shown this mechanism leads to self-propulsion orthogonal to the translational oscillatory motion, the question of whether this will be effective at higher Reynolds numbers remains. This work shows that the wake becomes three dimensional at a Reynolds number of approximately 100 due to a three-dimensional instability with a spanwise wavelength of approximately two cylinder diameters. The Floquet analysis shows that the two-dimensional base flow is also unstable to another three-dimensional instability with a shorter wavelength ($\lambda \approx 0.7D$) for $\mathrm{Re} \geq 226$; however, the experimental results, even at much higher Reynolds numbers do not show any sign of the occurrence of this mode. The experimental results indicate that the development of three dimensionality in the wake leads to significant distortion of the previously two-dimensional wake. The effect on the self-propulsion is yet to be determined.

ACKNOWLEDGMENTS

M.N. would like to acknowledge the support of a Monash Graduate Scholarship (MGS) and a Monash International Postgraduate Research Scholarship (MIPRS). D.L. acknowledges support from ARC Discovery under Grant No. DP0774525 and computing time from the Australian Partnership for Advanced Computing (APAC).

[1]P. W. Bearman, J. M. R. Graham, P. Naylor, and E. D. Obasaju, "The role of vortices in oscillatory flow about bluff cylinders," *International Symposium on Hydrodynamics in Ocean Engineering* (Norwegian Hydrodynamics Laboratories, Trondheim, 1981), pp. 621–635.
[2]H. M. Blackburn, J. R. Elston, and J. Sheridan, "Bluff-body propulsion produced by combined rotary and translational oscillation," Phys. Fluids **11**, 4 (1999).
[3]H. Honji, "Streaked flow around an oscillating cylinder," J. Fluid Mech. **107**, 509 (1981).
[4]C. H. K. Williamson, "Sinusoidal flow relative to circular cylinders," J. Fluid Mech. **155**, 141 (1985).
[5]M. Tatsuno and P. W. Bearman, "A visual study of the flow around an oscillating circular cylinder at low Keulegan–Carpenter numbers and low Stokes numbers," J. Fluid Mech. **211**, 157 (1990).
[6]P. Justesen, "A numerical study of oscillating flow around a circular cylinder," J. Fluid Mech. **222**, 157 (1991).
[7]G. Iliadis and G. Anagnostopoulos, "Viscous oscillatory flow around a circular cylinder at low Keulegan–Carpenter numbers and frequency parameters," Int. J. Numer. Methods Fluids **26**, 403 (1998).
[8]H. Dütsch, F. Durst, S. Becker, and H. Lienhart, "Low-Reynolds-number flow around an oscillating circular cylinder at low Keulegan–Carpenter numbers," J. Fluid Mech. **360**, 249 (1998).
[9]S. Taneda, "Visual observations of the flow past a circular cylinder performing a rotary oscillation," J. Phys. Soc. Jpn. **45**, 1038 (1978).
[10]P. T. Tokumaru and P. E. Dimotakis, "Rotary oscillation control of a cylinder wake," J. Fluid Mech. **224**, 77 (1991).
[11]P. Poncet, "Topological aspects of three-dimensional wakes behind rotary oscillating cylinders," J. Fluid Mech. **517**, 27 (2004).
[12]B. Thiria, S. Goujon-Durand, and J. E. Wesfreid, "The wake of a cylinder performing rotary oscillations," J. Fluid Mech. **560**, 123 (2006).
[13]S. J. Lee and J. Y. Lee, "Temporal evolution of wake behind a rotationally oscillating circular cylinder," Phys. Fluids **19**, 105104 (2007).
[14]T. Sarpkaya, "Force on a circular cylinder in viscous oscillatory flow at low Keulegan-Carpenter numbers," J. Fluid Mech. **165**, 61 (1986).
[15]J. R. Elston, J. Sheridan, and H. M. Blackburn, "Two-dimensional Floquet stability analysis of the flow produced by an oscillating circular cylinder in quiescent fluids," Eur. J. Mech. B/Fluids **23**, 99 (2004).
[16]J. R. Elston, H. M. Blackburn, and J. Sheridan, "The primary and secondary instabilities of flow generated by an oscillating circular cylinder," J. Fluid Mech. **550**, 359 (2006).
[17]J. S. Leontini, M. C. Thompson, and K. Hourigan, "Three-dimensional transition in the wake of a transversely oscillating cylinder," J. Fluid Mech. **577**, 79 (2007).
[18]D. Nehari, V. Armenio, and F. Ballio, "Three-dimensional analysis of the unidirectional oscillatory flow around a circular cylinder at low Keulegan–Carpenter and β numbers," J. Fluid Mech. **520**, 157 (2004).
[19]X.-Y. Lu and J. Sato, "A numerical study of flow past a rotationally oscillating circular cylinder," J. Fluids Struct. **10**, 829 (1996).
[20]M.-H. Chou, "Synchronization of vortex shedding from a cylinder under rotary oscillation," Comput. Fluids **26**, 755 (1997).
[21]Q. M. Al-Mdallal, "Analysis and computation of the cross-flow past an oscillating cylinder with two degrees of freedom," Ph.D. thesis, Memorial University of Newfoundland, 2004.
[22]S. Kocabiyik and Q. M. Al-Mdallal, "Bluff-body flow created by combined rotary and translational oscillation," in *Fluid Structure Interaction and Moving Boundary Problems*, WIT Transactions on the Built Environment, Vol. 84, edited by S. Chakrabarti (WIT, Southampton, 2005), p. 195.
[23]M. Nazarinia, D. Lo Jacono, M. C. Thompson, and J. Sheridan, "Flow behind a cylinder forced by a combination of oscillatory translational and rotational motions," Phys. Fluids **21**, 051701 (2009).
[24]J. R. Elston, "The structures and instabilities of flow generated by an oscillating circular cylinder," Ph.D. thesis, Monash University, 2005.
[25]J. Lighthill, "Fundamentals concerning wave loading on offshore structures," J. Fluid Mech. **173**, 667 (1986).
[26]P. K. Stansby, "The effect of end plates on the base pressure coefficient of a circular cylinder," Aeronaut. J. **78**, 36 (1974).
[27]R. J. Adrian, "Particle-imaging techniques for experimental fluid mechanics," Annu. Rev. Fluid Mech. **23**, 261 (1991).
[28]A. Fouras, D. Lo Jacono, and K. Hourigan, "Target-free stereo PIV: A novel technique with inherent error estimation and improved accuracy," Exp. Fluids **44**, 317 (2008).
[29]A. Fouras and J. Soria, "Accuracy of out-of-plane vorticity measurements derived from in-plane velocity field data," Exp. Fluids **25**, 409 (1998).
[30]G. E. Karniadakis and S. J. Sherwin, *Spectral/hp Methods for Computational Fluid Dynamics* (Oxford University Press, Oxford, 2005).
[31]M. C. Thompson, K. Hourigan, and J. Sheridan, "Three-dimensional instabilities in the wake of a circular cylinder," Exp. Therm. Fluid Sci. **12**, 190 (1996).
[32]G. Sheard, M. C. Thompson, and K. Hourigan, "From spheres to circular cylinders: The stability and flow structures of bluff ring wakes," J. Fluid Mech. **492**, 147 (2003).
[33]K. Ryan, M. C. Thompson, and K. Hourigan, "Three-dimensional transition in the wake of bluff elongated cylinders," J. Fluid Mech. **538**, 1 (2005).
[34]D. Lo Jacono, J. N. Sørensen, M. C. Thompson, and K. Hourigan, "Control of vortex breakdown in a closed cylinder with a small rotating rod," J. Fluids Struct. **24**, 1278 (2008).
[35]G. E. Karniadakis, M. Israeli, and S. A. Orszag, "High-order splitting methods of the incompressible Navier–Stokes equations," J. Comput. Phys. **97**, 414 (1991).
[36]M. C. Thompson, K. Hourigan, A. Cheung, and T. Leweke, "Hydrodynamics of a particle impact on a wall," Appl. Math. Model. **30**, 1356 (2006).
[37]C. Canuto, M. Hussaini, A. Quarteroni, and T. Zang, *Spectral Methods in Fluid Dynamics*, 2nd ed. (Springer-Verlag, Berlin, 1990).
[38]D. Barkley and R. D. Henderson, "Three-dimensional Floquet stability analysis of the wake of a circular cylinder," J. Fluid Mech. **322**, 215 (1996).
[39]B. R. Morton, "The generation and decay of vorticity," Geophys. Astrophys. Fluid Dyn. **28**, 277 (1984).
[40]C. H. K. Williamson, "The existence of two stages in the transition to three–dimensionality of a circular cylinder wake," Phys. Fluids **31**, 3165 (1988).
[41]H. M. Blackburn, F. Marques, and J. M. Lopez, "Symmetry breaking of two-dimensional time-periodic wakes," J. Fluid Mech. **522**, 395 (2005).
[42]J. Wu, J. Sheridan, M. C. Welsh, and K. Hourigan, "Three-dimensional vortex structures in a cylinder wake," J. Fluid Mech. **312**, 201 (1996).
[43]C. H. K. Williamson, "Three-dimensional wake transition," J. Fluid Mech. **328**, 345 (1996).